The Combination of Charge and Energy Transfer Processes in MOF for Efficient Photocatalytic Oxidative Coupling of Amines

Feng-Juan Zhao,[†,‡] *Guoliang Zhang,*[§] *Zhanfeng Ju,*[†] *Yan-Xi Tan,**[,†] *and Daqiang Yuan**[,†,‡]

[†]State Key Laboratory of Structural Chemistry, Fujian Institute of Research on the Structure of Matter, Chinese Academy of Sciences, Fuzhou, 350002, Fujian, China.

[‡]Fujian Normal University, Cangshan Campus, No.8 Shangsan Road, Cangshan District, Fuzhou, 350007, Fujian, China.

[§]School of mechanical engineering, Tianjin University of Technology and Education, Tianjin, 300222, China

E-mail: tyx@fjirsm.ac.cn; ydq@fjirsm.ac.cn

X-ray crystallography: Single-crystal X-ray diffraction data were collected on a SuperNova diffractometer equipped with a Cu Kα radiation (λ = 1.5406 Å) and an Atlas CCD detector under 150 K. The structures were solved by using the direct method and refined by full-matrix least-squares methods on F^2 by using the SHELX-2017 program package. All non-hydrogen atoms were refined anisotropically. In order to obtain a clear structure, we used the *SQUEEZE* instruction of *PLATON* to remove the contribution of disordered guest molecules and refined further using the data generated.

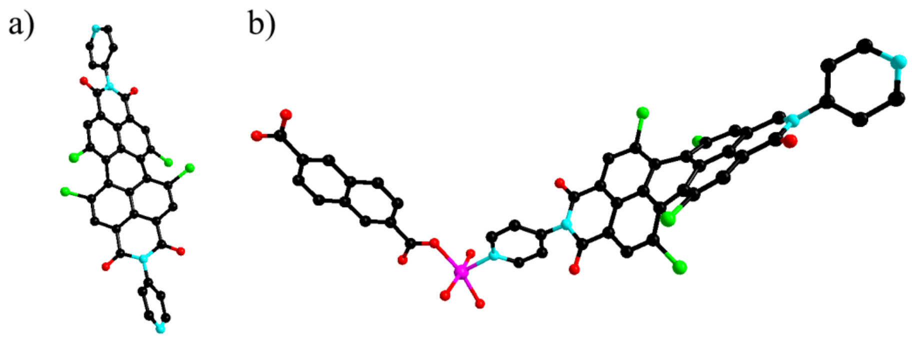

Figure. S1. (a) The structure of *bis(N-pyridyl) tetrachloroperylene peryleneimide (L)* and (b) the structure of **FJI-Y10** asymmetric unit.

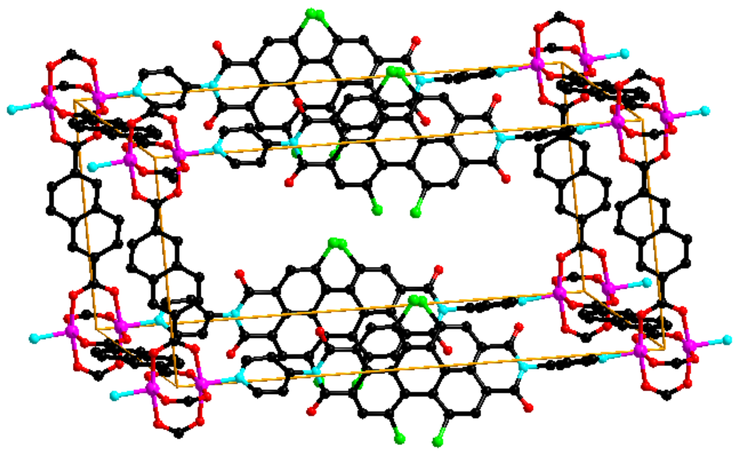

Figure. S2. The internal framework Co···Co distance is up to 13.0769-23.6816 Å.

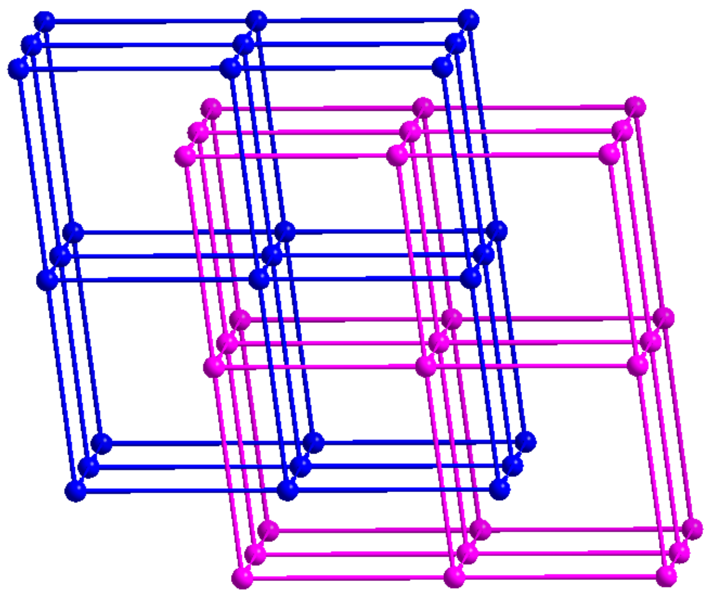

Figure. S3. The 6-connected *pcu* net of **FJI-Y10**.

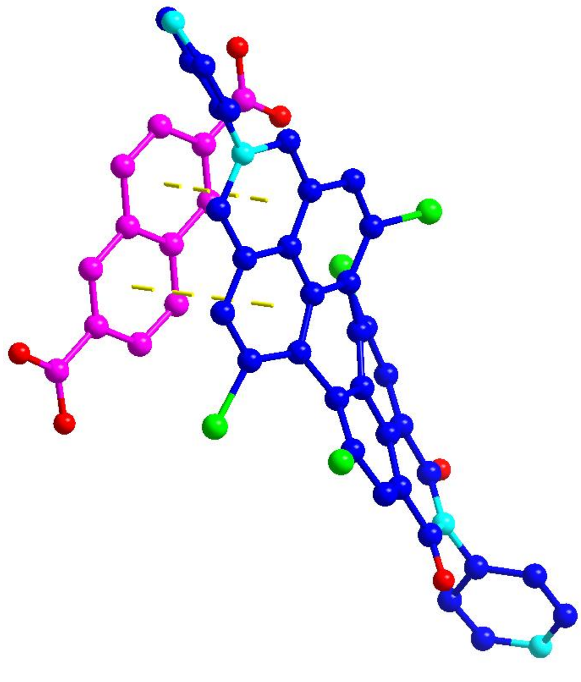

Figure. S4. There are face-to-face π···π stacking with the distance of 3.5187 to 3.7444 Å between the phenyl rings of L and 2,6-NDC ligands from different *pcu* lattices.

1. Gas adsorption

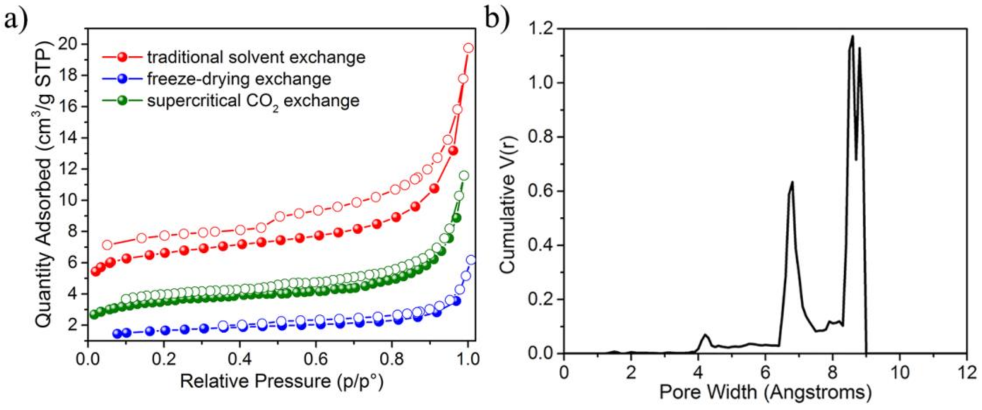

Figure. S5. (a) N_2 sorption measurements at 77 K for **FJI-Y10** by adopting traditional solvent (CH_3CN) exchange (red) and freeze-drying (blue) and supercritical CO_2 exchange (green). (b) The pore size distribution of **FJI-Y10** simulated by Zeo++.

2. PXRD

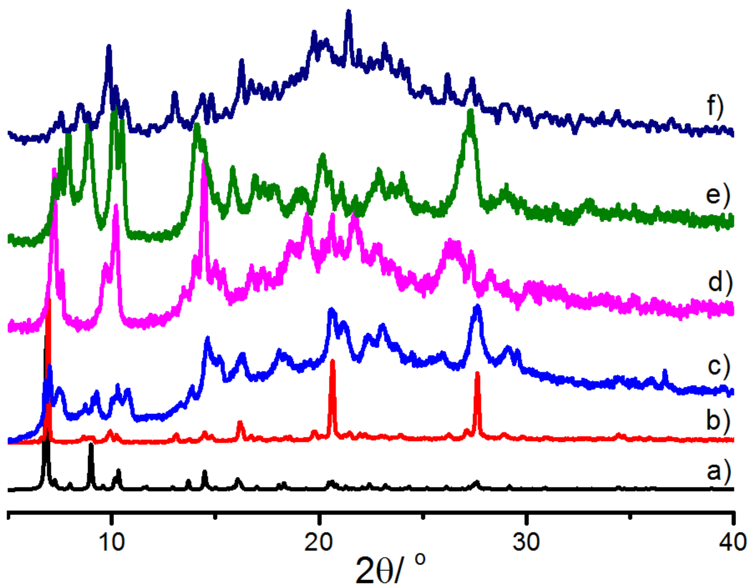

Figure. S6. PXRD patterns of **FJI-Y10**: simulate one (a), as-synthesized sample (b), sample after catalysis (c), sample activated by traditional MeCN-exchange (d), sample activated by freeze-drying (e), sample activated by supercritical CO_2 exchange (f).

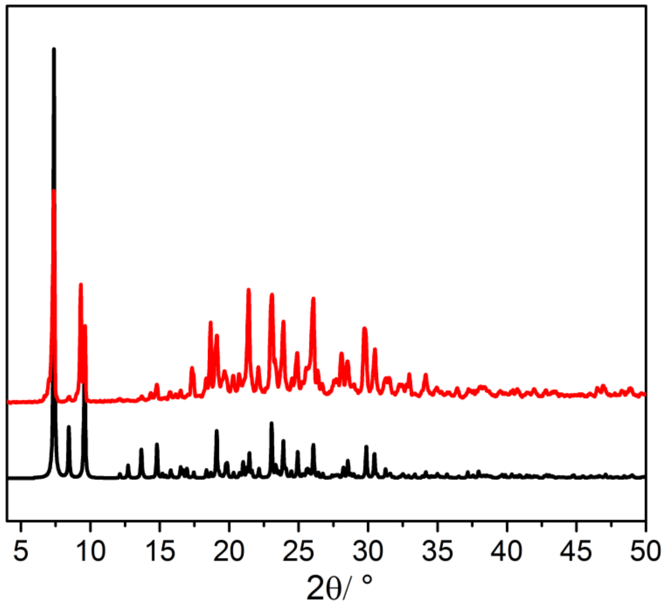

Figure. S7. PXRD patterns of the simulate one (black) and as-synthesized *bis(N-pyridyl) tetrachloroperylene peryleneimide (L)* (red).

3. TGA

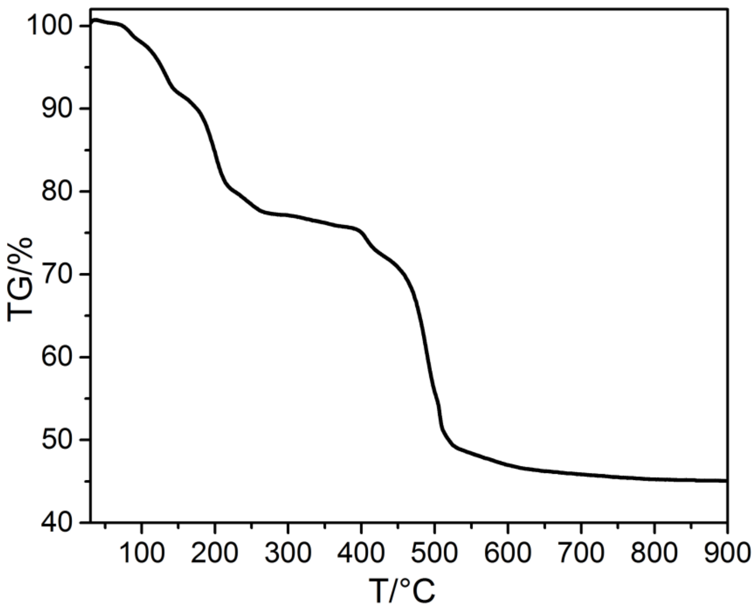

Figure. S8. TGA curve for **FJI-Y10**.

4. UV-Vis

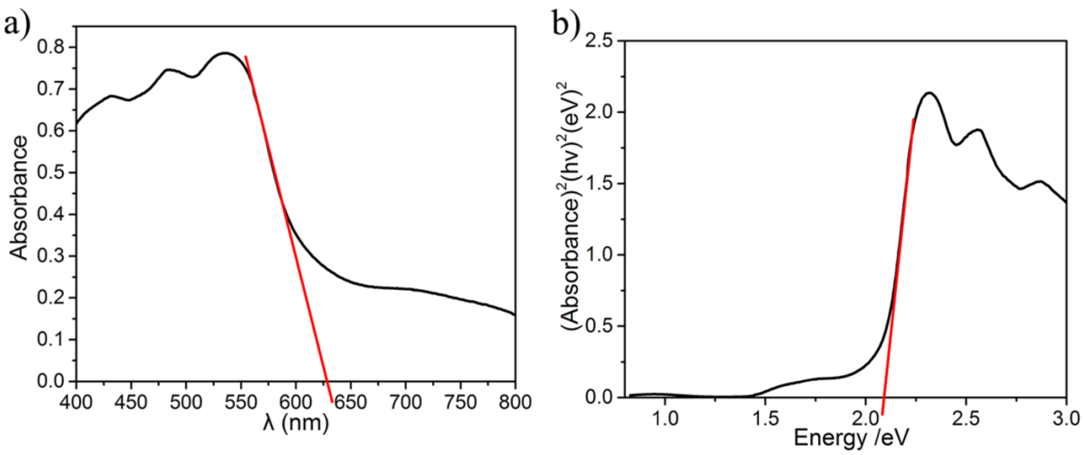

Figure. S9. (a) UV-visible diffuse reflectance spectra of **FJI-Y10** and (b) plot of Kubelka–Munk function for the band-gap determination.

5. EPR

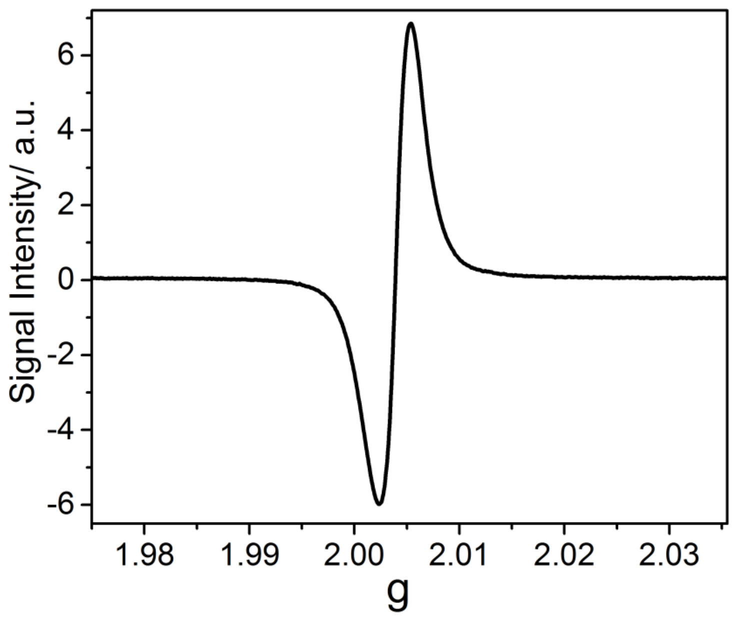

Figure. S10. EPR spectra of *bis(N-pyridyl) tetrachloroperylene peryleneimide (L)*.

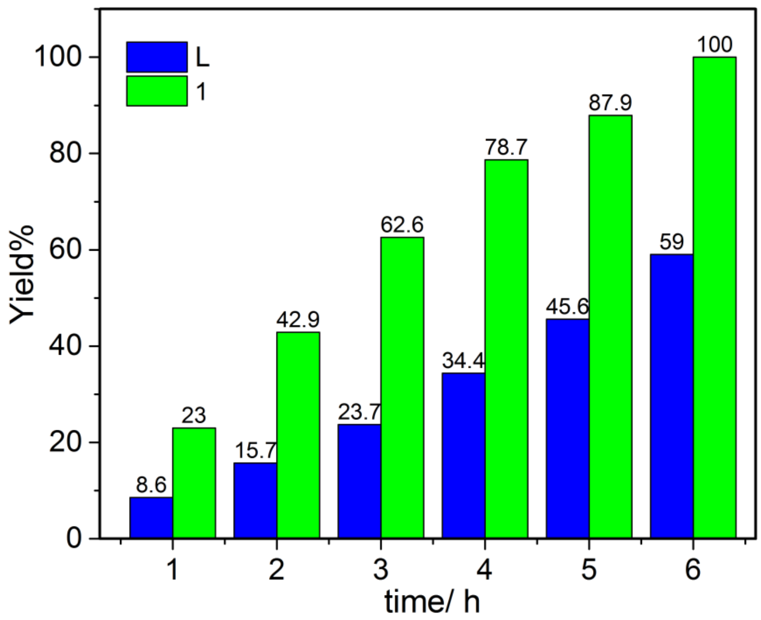

Figure. S11. Comparision of photocatalytic oxidation of benzamine coupling reaction rates of MOF **FJI-Y10** and L under the same test conditions.

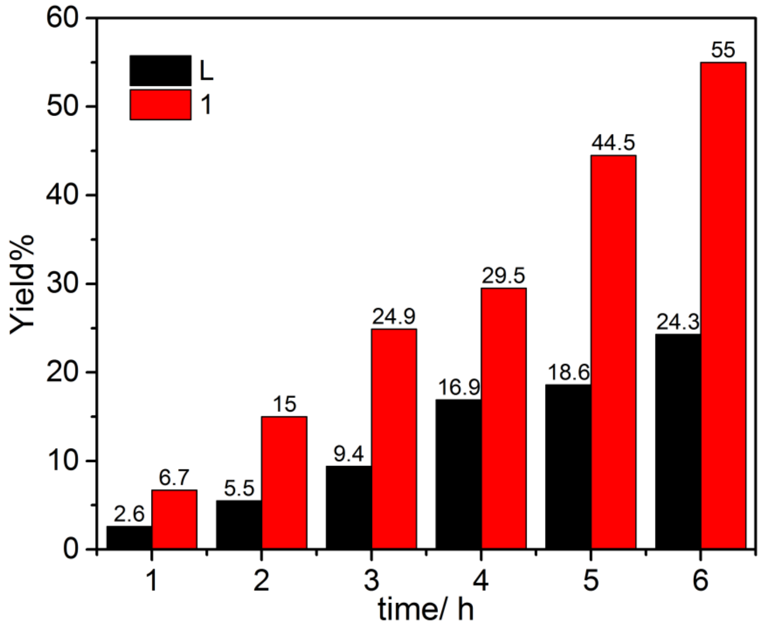

Figure. S12. Comparision of photocatalytic oxidation of heptylamine coupling reaction rates of MOF **FJI-Y10** and L under the same test conditions.

6. FT-IR spectra

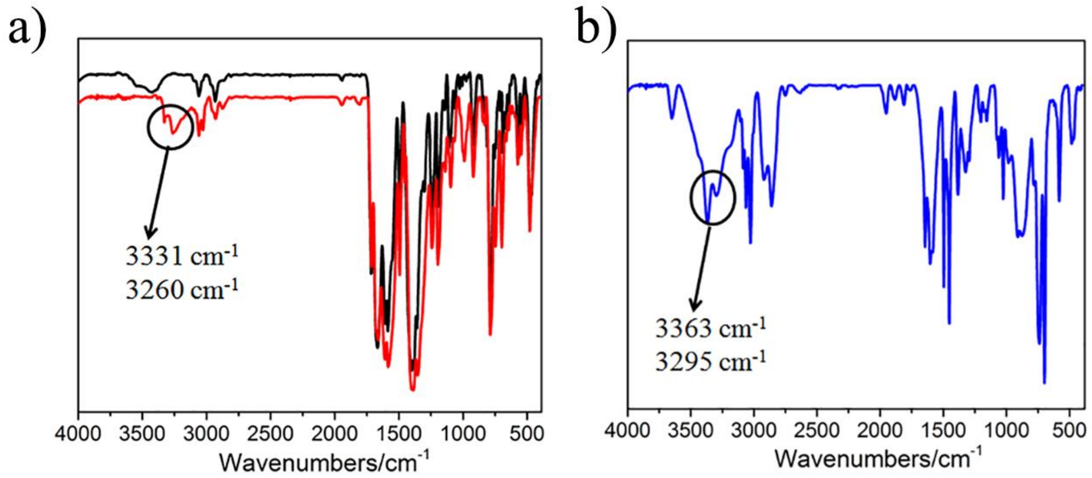

Figure. S13 (a) Infrared IR spectra of **FJI-Y10** (black line) and **FJI-Y10** obtained after the absorption of benzylamine (red line). (b) Infrared IR spectra of benzylamine.

7. Mott-Schottky measurements

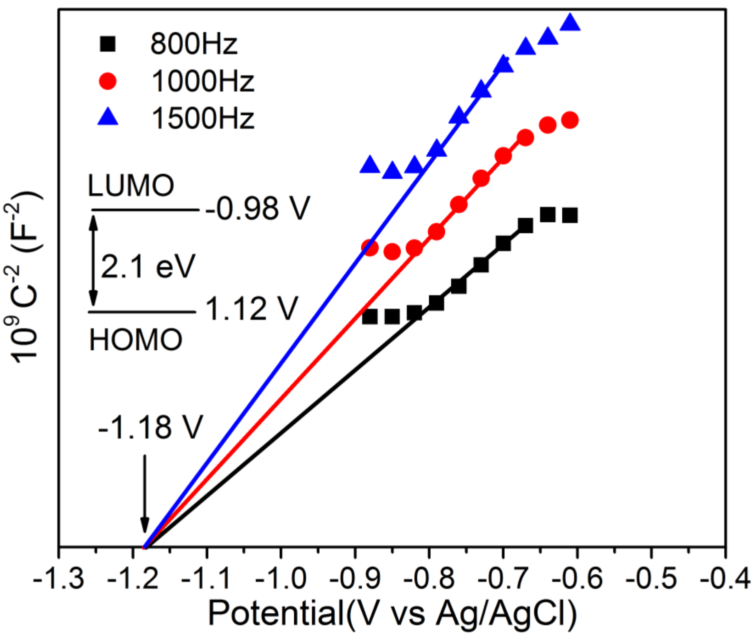

Figure. S14. Mott-Schottky plots for **FJI-Y10** at frequencies of 800, 1000 and 1500 Hz. The positive slope of the obtained C^{-2} values (vs the applied potentials) is consistent with that of the character of typical n-type semiconductors. (Inset: the HOMO and LUMO levels of **FJI-Y10**)

8. Photocurrent measurement

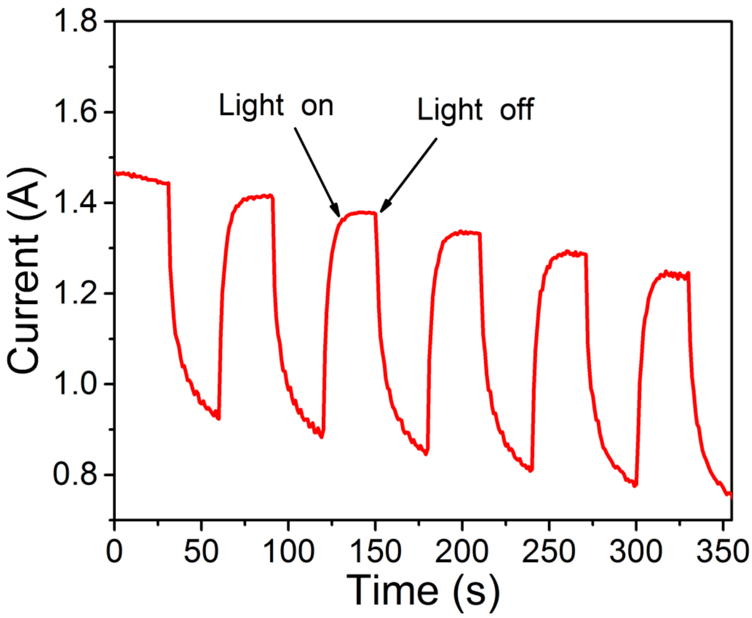

Figure. S15. Photocurrent responses for **FJI-Y10** photocatalysts.

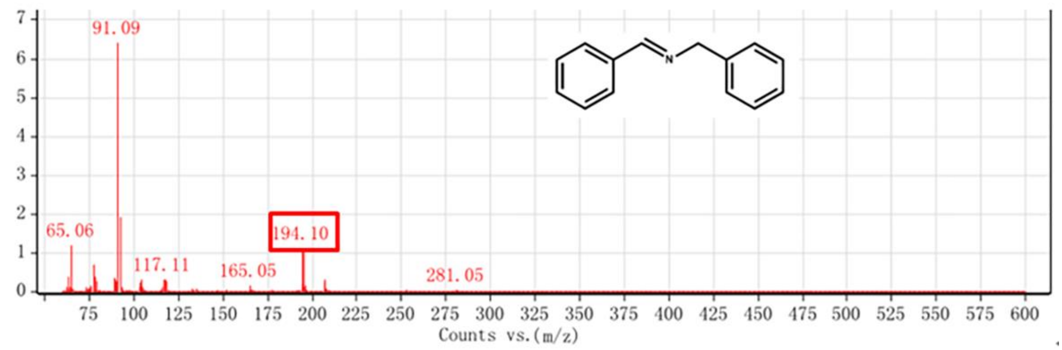

Figure. S16. MS spectrum of the reaction mixture after photo-reduction (entry 1 in Table 2).

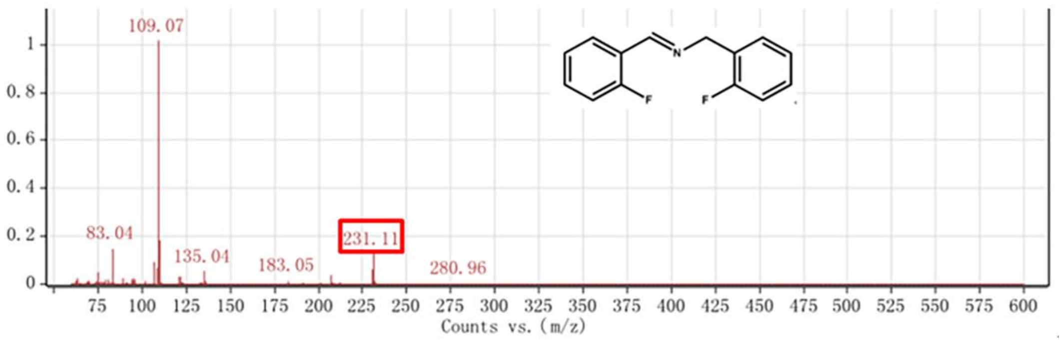

Figure. S17. MS spectrum of the reaction mixture after photo-reduction (entry 2 in Table 2).

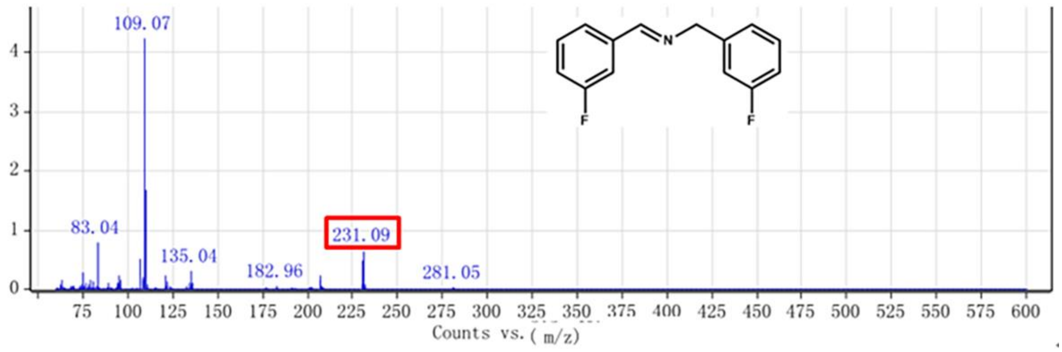

Figure. S18. MS spectrum of the reaction mixture after photo-reduction (entry 3 in Table 2).

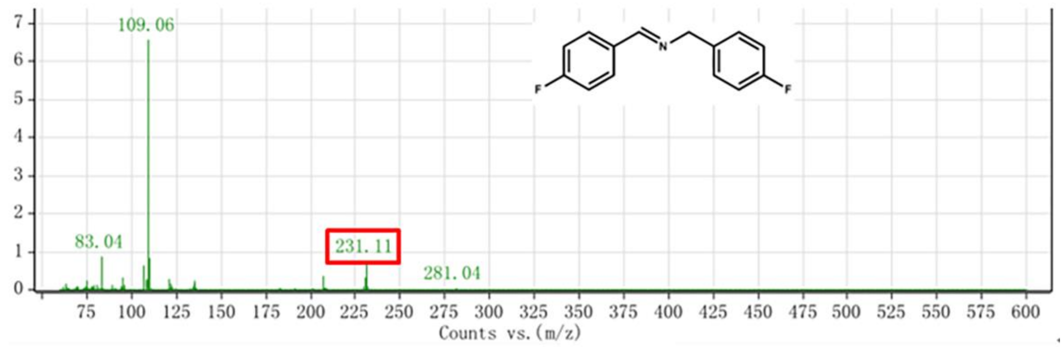

Figure. S19. MS spectrum of the reaction mixture after photo-reduction (entry 4 in Table 2).

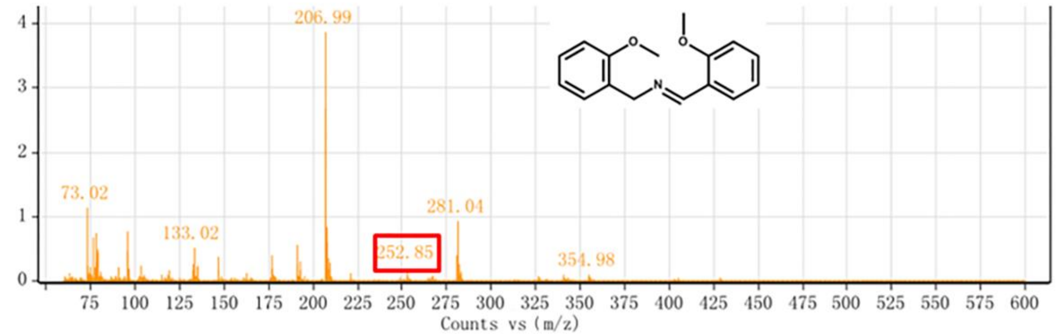

Figure. S20. MS spectrum of the reaction mixture after photo-reduction (entry 5 in Table 2).

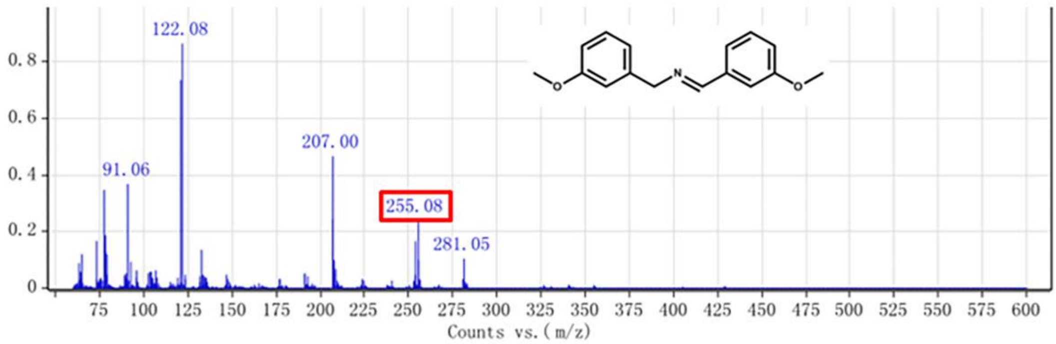

Figure. S21. MS spectrum of the reaction mixture after photo-reduction (entry 6 in Table 2).

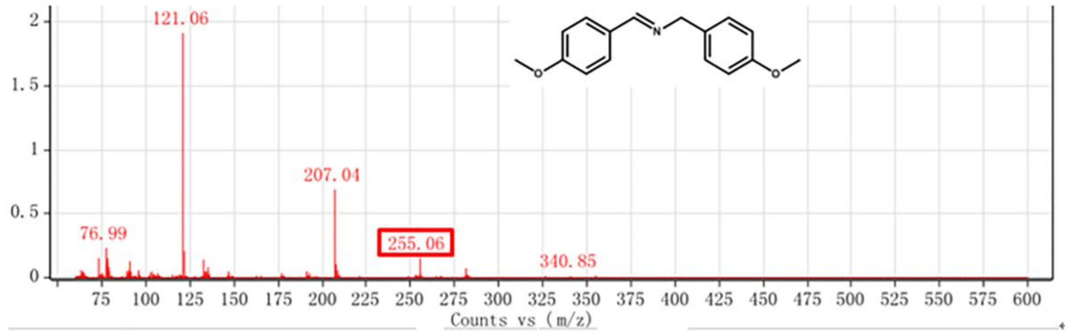

Figure. S22. MS spectrum of the reaction mixture after photo-reduction (entry 7 in Table 2).

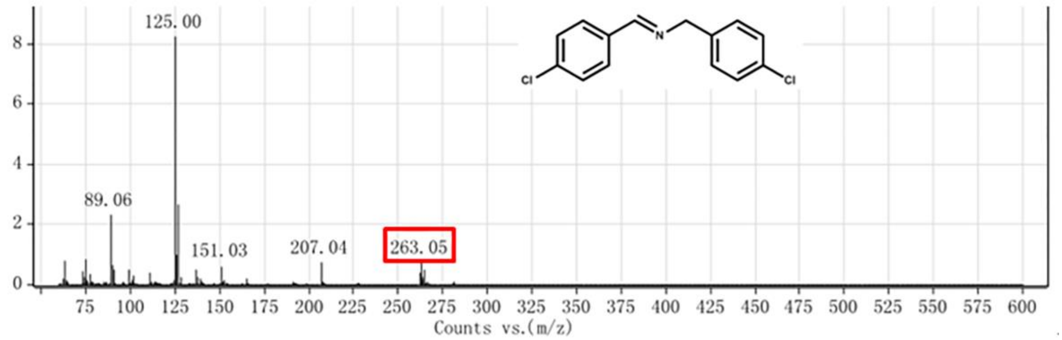

Figure. S23. MS spectrum of the reaction mixture after photo-reduction (entry 8 in Table 2).

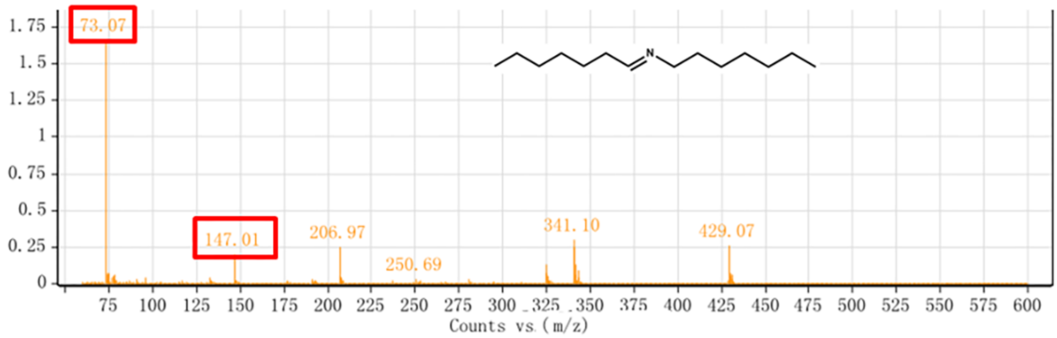

Figure. S24. MS spectrum of the reaction mixture after photo-reduction (entry 9 in Table 2).